Molecular Biology of the Cell
Vol. 15, 3631–3641, August 2004

# Cholera Toxin Toxicity Does Not Require Functional Arf6- and Dynamin-dependent Endocytic Pathways[D] [V]

**Ramiro H. Massol,* Jakob E. Larsen,* Yukako Fujinaga,† Wayne I. Lencer,† and Tomas Kirchhausen*‡**

*Department of Cell Biology, Harvard Medical School and The Center for Blood Research for Biomedical Research, Boston, Massachusetts 02115; and †Gastrointestinal Cell Biology, Department of Pediatrics, Children's Hospital and Harvard Medical School and the Harvard Digestive Diseases Center, Boston, Massachusetts 02115

Submitted April 5, 2004; Accepted April 29, 2004
Monitoring Editor: Suzanne Pfeffer

**Cholera toxin (CT) and related $AB_5$ toxins bind to glycolipids at the plasma membrane and are then transported in a retrograde manner, first to the Golgi and then to the endoplasmic reticulum (ER). In the ER, the catalytic subunit of CT is translocated into the cytosol, resulting in toxicity. Using fluorescence microscopy, we found that CT is internalized by multiple endocytic pathways. Inhibition of the clathrin-, caveolin-, or Arf6-dependent pathways by overexpression of appropriate dominant mutants had no effect on retrograde traffic of CT to the Golgi and ER, and it did not affect CT toxicity. Unexpectedly, when we blocked all three endocytic pathways at once, although fluorescent CT in the Golgi and ER became undetectable, CT-induced toxicity was largely unaffected. These results are consistent with the existence of an additional retrograde pathway used by CT to reach the ER.**

## INTRODUCTION

Bacterial and plant protein exotoxins are among the most lethal factors produced in nature. Some act on the cell surface by perturbing signaling pathways or by disrupting the integrity of the plasma membrane, whereas others exploit membrane traffic pathways to gain access to their cytosolic targets (Montecucco, 1998; Sandvig and van Deurs, 2002a,b). A well-characterized toxin of this latter group is cholera toxin (CT), produced by *Vibrio cholerae*. CT belongs to the AB family of bacterial exotoxins and consists of a pentameric B subunit and an A subunit comprising two polypeptides, A1 and A2, linked by a disulfide bond. The B subunit binds with high affinity and specificity to GM1, a ganglioside present in apical membranes of all intestinal epithelial cells. The A1 polypeptide has ADP-ribosylase activity, whereas A2 contains a carboxy-terminal KDEL ER retrieval signal.

CT first binds to GM1 at the apical surface of jejunal intestinal cells and then follows a complex endocytic pathway involving retrograde membrane traffic through the Golgi complex to the ER (Joseph *et al.*, 1978; Joseph *et al.*, 1979; Lencer *et al.*, 1993; Nambiar *et al.*, 1993; Orlandi *et al.*, 1993; Lencer *et al.*, 1995; Majoul *et al.*, 1996; Majoul *et al.*, 1998; Fujinaga *et al.*, 2003). Binding to GM1 associates CT with detergent-resistant membranes, presumably lipid rafts; the CT–ganglioside complex then moves from the plasma membrane to the ER (Fujinaga *et al.*, 2003). Other toxins and some viruses also bind to glycolipids to enter the ER and cause disease (Falguieres *et al.*, 2001; Pelkmans *et al.*, 2001, 2002; Tsai *et al.*, 2003). In CT, the A1 peptide is unfolded in the ER lumen and retrotranslocated by the Sec61p complex into the cytosol (Schmitz *et al.*, 2000; Tsai *et al.*, 2001, 2002), where it catalyzes the ADP-ribosylation of the heterotrimeric stimulatory G protein (Gsα), permanently activating adenylate cyclase (Kahn and Gilman, 1984; Van Dop *et al.*, 1984; Moss and Vaughan, 1988). The resulting increase in intracellular cAMP (Schafer *et al.*, 1970; Kassis and Fishman, 1982; Kassis *et al.*, 1982) causes net intestinal salt and water secretion, resulting in massive secretory diarrhea (Spangler, 1992), and changes in cell morphology (Guerrant *et al.*, 1974; Donta *et al.*, 1976; Barbieri *et al.*, 2002) presumably due to activation of cAMP-dependent protein kinase A (Diviani and Scott, 2001; Scott, 2003).

Exactly how the CT–GM1 complex traffics from the plasma membrane to the Golgi and then to the ER remains unknown. One possibility is that the toxin-GM1 complex is primarily carried to the ER by using a caveolin-dependent retrograde trafficking pathway (Hagmann and Fishman, 1982; Montesano *et al.*, 1982; Tran *et al.*, 1987; Parton, 1994; Mobius *et al.*, 1999; Badizadegan *et al.*, 2000; Fujinaga *et al.*, 2003). Cholesterol depletion, or absence of endogenous caveolin (Fishman and Atikkan, 1980; Orlandi and Fishman, 1998; Torgersen *et al.*, 2001; Wolf *et al.*, 2002; Fujinaga *et al.*, 2003), or caveolin depletion by RNA interference (Nichols, 2002), however, do not completely prevent CT uptake or toxicity, with the exception of the work by Orlandi and Fishman (1998) who found a complete block in cAMP production by CT in response to filipin. It also has been proposed that CT may enter cells via the clathrin-dependent pathway, but inhibition of this pathway by chemical or genetic treatments results in only a partial decrease in CT uptake (Sofer and Futerman, 1995; Nichols *et al.*, 2001; Shogomori and Futerman, 2001; Torgersen *et al.*, 2001). A third possible entry pathway not yet directly addressed is the one regulated by the small GTPase Arf6. This pathway is

Article published online ahead of print. Mol. Biol. Cell 10.1091/mbc.E04–04–0283. Article and publication date are available at www.molbiolcell.org/cgi/doi/10.1091/mbc.E04–04–0283.

[D] [V] Online version of this article contains supporting material. Online version is available at www.molbiolcell.org.

‡ Corresponding author. E-mail address: kirchhausen@crystal.harvard.edu.

© 2004 by The American Society for Cell Biology

functionally linked to EHD1 (Caplan *et al*., 2002) and is used by several proteins (major histocompatibility complex [MHC] class I, interleukin 2 receptor, carboxypeptidase E, and β1 integrin receptor) that traffic between plasma membrane and endosomes (Radhakrishna and Donaldson, 1997; Brown *et al*., 2001; Blagoveshchenskaya *et al*., 2002; Arnaoutova *et al*., 2003). It is also possible that CT shows no preference for any given entry route and instead uses a combination of these pathways to arrive at the endosomal and Golgi compartments.

With the goal of determining the relative contribution of these entry routes in CT transport to the ER, we measured toxin transport by imaging fluorescent CT, and toxin-induced activation of adenylyl cyclase by scoring CT-induced changes in cell shape while interfering specifically with clathrin-, caveolin-, or Arf6-dependent endocytosis alone, or all three pathways together. Inhibition of the caveolin, clathrin, or Arf6 pathways alone had minimal effects on CT entry, whereas the simultaneous block of entry through all these three pathways lead to a substantial reduction of at least 100-fold in the steady-state accumulation of CT in the endosomal and Golgi compartments. Unexpectedly, the combined inhibition of clathrin, caveolin, and Arf6 endocytic pathways had minimal effects on CT-induced toxicity. Based on these results, we suggest that an additional route for CT entry that is dynamin and Arf6 independent and of sufficient transport capacity exists to allow toxin access to the ER.

## MATERIALS AND METHODS

### *Reagents*

The following reagents were used: latrunculin A, nocodazole, and wild-type cholera toxin (Calbiochem, San Diego, CA); methyl-β-cyclodextrin, phorbol 12-myristate 13-acetate (PMA), genistein, brefeldin A (BFA), forskolin, and 8-Br-cAMP (Sigma-Aldrich, St. Louis, MO); geneticin (Invitrogen, Carlsbad, CA); and BODIPY FL-C5-ganglioside fluorescent GM1 lipids (Molecular Probes, Eugene, OR).

### *Cells*

BSC1 monkey kidney epithelial cells (ATCC CCL-26), and Y-1 mouse adrenal cells (ATCC CCL-79) were grown in DMEM or RPMI 1640 medium, respectively, supplemented with 10% fetal bovine serum, 2 mM L-glutamine, penicillin (50 U/ml), streptomycin (50 mg/ml), and nonessential amino acids (0.1 mM). Most morphological studies were performed with the larger BSC1 cells; Y-1 cells were used for the toxicity assay due to their fast and striking change in shape after a CT-induced increase in cAMP. For CT traffic studies, cells were grown on coverslips (18- or 25-mm sterile coverslips) to 50–70% confluence. For live-cell imaging studies of CT access to the Golgi complex, we generated a clone of BSC1 cells stably expressing a chimera comprised of the Golgi sorting signal of galactosyltransferase fused to enhanced green fluorescent protein (EGFP) (BSC1/GalT-EGFP). We made the expression vector by subcloning GalT-EGFP from the pST-GalT-EGFP (kind gift from Dr. Jennifer Lippincott-Schwartz, National Institutes of Health, Bethesda, MD) into the pEGFP-N1 vector (BD Biosciences Clontech, Palo Alto, CA).

### *Transfection*

Hemagglutinin (HA) and EGFP-tagged constructs of the dynamin 1 and 2 dominant negative mutants K44A (DynK44A), respectively, were kind gifts from Dr. Sandra Schmid (The Scripps Research Institute, La Jolla, CA). Human HA-tagged Arf6 (wild type, T27N, or Q67L) plasmids were kind gifts from Dr. Julie Donaldson (National Institutes of Health), and Dr. Michel Franco (Institut dePharmacologie Moléculaire et Cellulaire, Centre National de la Recherche Scientifique, Valbonne, France). Dr Jeffrey Pessin (University of Iowa, Iowa City, IA) generously provided plasmids encoding myc-tagged caveolin 1 wild type, and mutants S80E and S80A. Two other myc-tagged mutants of caveolin 1 [Cav1(KSF) and Cav1(DGI)] were generated based on previously reported mutants of Cav3 (Luetterforst *et al*., 1999). Briefly, after protein homology alignment of the full-length wild-type caveolin 1 and 3 sequences, *Eco*RI restriction sites followed by Kozak sequences and start codons before positions K135 or D82 were incorporated by site-directed mutagenesis (QuikChange; Stratagene, La Jolla, CA) into full-length caveolin 1. The resulting N terminus-truncated mutants were cloned into pCDNA3-myc-his and verified by sequencing. Dr. Jennifer Lippincott-Schwartz kindly provided a plasmid encoding EGFP-Eps15Δ95–295 fused to EGFP. The major histocompatibility complex (MHC) class I HLA-A2 fused to EGFP (EGFP-MHC-I) in its ectodomain was a kind gift from Dr. Domenico Tortorella (Harvard Medical School, Boston, MA). The EHD1 cDNA (a kind gift from Dr. Mia Horowitz, Tel Aviv University, Tel Aviv, Israel) was fused with EGFP in the pEGFP-C1 vector (BD Biosciences Clontech) to obtain EGFP-EHD1. The rat light chain A1 subunit of clathrin (Kirchhausen *et al*., 1987) was fused to EYFP in the pEGFP-C1 vector to obtain EYFP-LCA. All transfections were carried out using FuGENE 6 (Roche Diagnostics, Indianapolis, IN), and cells were evaluated 24–48 h later.

### *CT Uptake*

The traffic studies were performed using a mutant of CT, E112D, that is poorly able to catalyze the ADP-ribosylation of substrates (Jobling and Holmes, 2001). To render CT(E112D) fluorescent, this protein was first bound to galactose beads, to protect the lysine residues of the GM1 binding domains of CT, and then fluorescently labeled with Alexa Fluor 594 following the instructions of the manufacturer (Molecular Probes), obtaining a degree of labeling of ~1.2 moles of dye per mole of protein. For simplicity, we refer to the Alexa 594-labeled CT(E112D) as CT(E112D) from here on. Functional tests in Y-1 cells by using fluorescently labeled CT(E112D) at very high concentrations (>40 nM) demonstrated that this toxin still maintains a low toxicity (our unpublished data), indicating that the addition of fluorophores did not modify the binding and traffic properties of CT.

Continuous uptake of CT was performed by loading BSC1 or Y-1 cells with 20 nM CT(E112D) in minimal essential medium supplemented with 20 mM HEPES and 0.5 g% bovine serum albumin (HMEMB) at 37°C for different times (20–150 min). Cells were washed and fixed or transferred to a live-cell imaging chamber for time-lapse recording. Alternatively, CT(E112D) was bound at 4°C for 30 min before removing the unbound toxin and shifting to 37°C. We followed the real-time uptake of CT by replacing the medium in the temperature-controlled chamber with 37°C prewarmed medium containing 30 nM CT.

### *Antibody Staining of BSC1 Cells*

Cells were fixed in 3% paraformaldehyde (PFA) in phosphate-buffered saline (PBS) for 10 min at room temperature (RT), washed with PBS supplemented with 1 mM $MgCl_2$ and 0.1 mM $CaCl_2$ ($PBS^{++}$), and excessive PFA reactive groups were quenched with 50 mM $NH_4Cl$ in $PBS^{++}$ for 15 min at RT. To prevent unspecific binding of antibodies, samples were incubated with 2% BSA in $PBS^{++}$ for 30 min at RT. All antibodies were diluted in HMEMB supplemented with 0.1 g% saponin. For microtubule staining we used a rat anti-α-tubulin monoclonal antibody (1:200; Oxford Biotechnology, Raleigh, NC) followed by goat anti-rat Cy3-labeled secondary antibody (Jackson ImmunoResearch Laboratories, West Grove, PA). A purified mouse monoclonal antibody (W6/32; hybridoma generously provided by Dr. Hidde Ploegh, Harvard Medical School), which recognizes assembled MHC-I heavy chain-β2 microglobulin complexes, was used for MHC-I-antibody feeding experiments. Staining for the early endosomal marker EEA1 or the AP-2 adaptor complex was performed with a goat polyclonal anti-EEA1 antibody (Santa Cruz Biotechnology, Santa Cruz, CA) or a rabbit polyclonal anti-β2 (produced in our laboratory), respectively. The *trans*-Golgi network (TGN) and the Golgi matrix were stained with a sheep anti-human TGN46 polyclonal antibody (Serotec, Raleigh, NC) or a mouse monoclonal anti-GM130 (BD Biosciences, San Jose, CA), respectively. HA and c-myc epitopes were detected using mouse monoclonal antibodies 12CA5 (harvested from hybridoma cells), and 9E10 (Santa Cruz Biotechnology), respectively. The antibody–epitope complexes were visualized by secondary staining with Alexa488, Alexa594, or Alexa647-goat anti-mouse antibodies (Molecular Probes).

### *cAMP-dependent Morphological Change Assay*

A single-cell based cAMP-dependent change in cell morphology assay was used to assess CT-induced toxicity. The assay relies on scoring the dramatic alteration in cellular morphology observed on cells attached to a substrate in response to an increase of intracellular cAMP levels. This assay was developed as a way to indirectly determine the levels of cAMP due to direct or indirect activation of adenylate cyclase (Kowal and Fiedler, 1969; Guerrant *et al*., 1974; Maneval *et al*., 1981; Maenhaut and Libert, 1990; Ulaner *et al*., 1999). Incubations with CT; forskolin, a direct activator of adenylate cyclase (Seamon and Daly, 1981; Seamon *et al*., 1981); or the cell-permeable cAMP analogues dibutyryl cAMP or 8-bromo-cAMP (8-Br-cAMP) elicited similar cell shape changes over the same period (Nambiar *et al*., 1993; Dong *et al*., 1998; Ulaner *et al*., 1999). It is presumed that the changes in cell shape depend on the activation of cAMP-dependent protein kinase influencing the actin cytoskeleton (reviewed by Diviani and Scott, 2001).

Y-1 adrenal cells were seeded at 20–30 × $10^4$ cells/well on 18-mm coverslips for 24 h and transfected or not with different plasmids encoding the proteins interfering with membrane traffic. Twenty-four hours later, the cells were washed with $PBS^{++}$ and then incubated with HMEMB medium with different concentrations of forskolin, CT holotoxin (wild type or E112D mutant), or CT B subunit for 1.5 h at 37°C. Inhibition of clathrin-dependent endocytosis was determined by visual inspection of fluorescent human transferrin (Tf) internalized during the last 15 min. Cells were fixed and processed

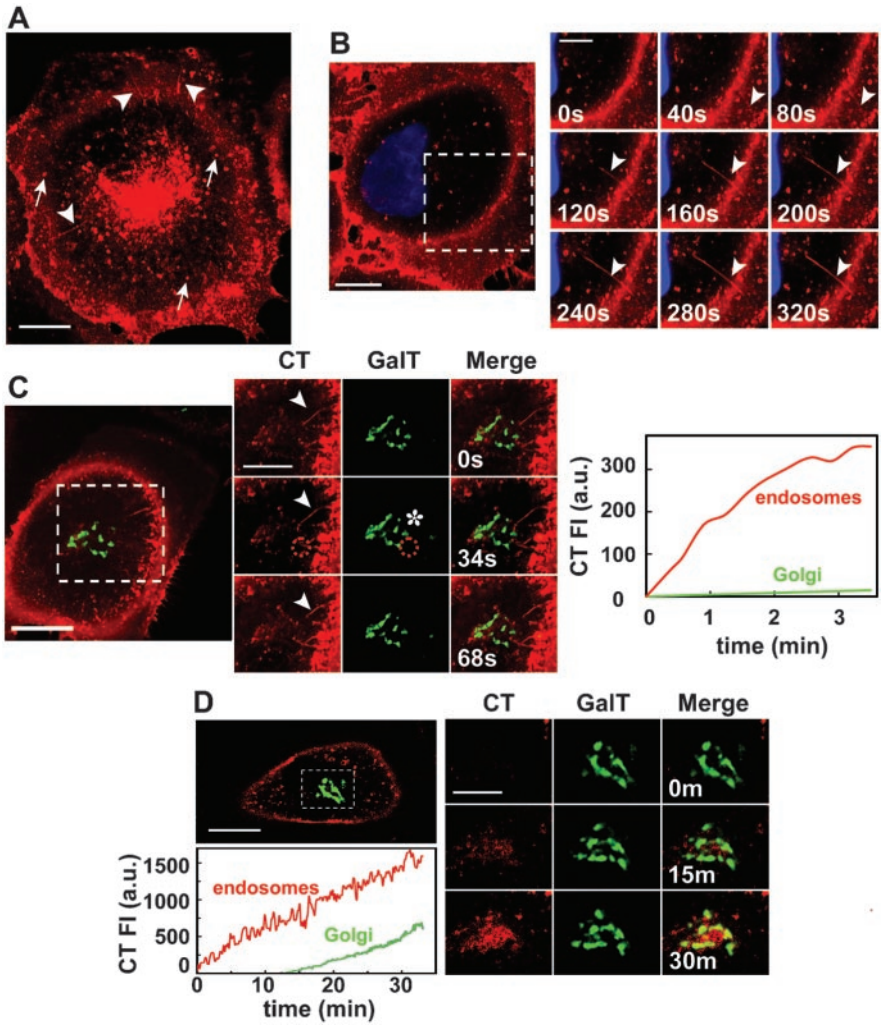


**Figure 1.** Vesicles and tubules internalize CT to a perinuclear endosomal compartment. (A) CT traffics in vesicles (arrows) and tubules (arrowheads) from the plasma membrane toward the perinuclear endosomal/Golgi area (Movie 1). BSC1 cells were incubated with 20 nM nontoxic mutant CT(E112D) labeled with Alexa594 (red) at 37°C for 45 min. (B) CT enters BSC1 cells via both vesicles and tubules (arrowheads). BSC1 cells were incubated with 20 nM CT(E112D) at 4°C for 30 min, shifted to 37°C for 2 min, and then the time course of toxin internalization was recorded (inset and Movie 3). Nucleus was stained with Hoechst (blue). (C) Endocytic tubules containing CT (arrowhead) extend from the cell surface toward a perinuclear endosomal compartment in close contact with the Golgi complex (GalT-EGFP, green). BSC1 cells were incubated as described in B. Selected snapshots of time course of CT internalization are shown. The plot shows the time course of CT appearance in endosomes (red line) within the indicated area (red stippled circle); after this brief uptake period, almost no CT reaches the Golgi, including the regions in proximity with the tubules (* in image and green line in plot). Colocalization of CT with the Golgi region was calculated by r analysis as explained in MATERIALS AND METHODS. (D) CT is first transported to endosomes before reaching the Golgi complex. CT(E112D) was added to BSC1/GalT-EGFP cells at 37°C during recording of time lapse. Selected snapshots are shown after 0, 15, and 30 min of CT addition. Colocalization of CT with the Golgi region (stippled box) was calculated as described in C. The plot shows the continuous accumulation of CT in endosomes (red line) and Golgi complex (green line). Bars, 20 $\mu$m (whole cell) and 10 $\mu$m (cropped areas).

for fluorescence microscopy. Random fields were imaged, and 100–300 cells were analyzed by phase contrast (all cells) and by fluorescence (transfected cells) microscopy. A change in morphology was scored when the cell looked rounded rather than flat and/or showed long processes. The fluorescent images corresponding to the transfected cells offered a simple and nonambiguous way to determine their cell shape, particularly in regions of relatively high cell density. Phase contrast images were used to confirm the scoring by using fluorescent images and to determine the effect of any given treatment in the surrounding nontransfected cells (internal control). All experiments were repeated at least four times.

### *Microscopy Data Acquisition and Processing*

Images were acquired and processed as described previously (Larsen *et al.*, 2004). The amount of CT localized in the trans-Golgi network (TGN)/Golgi compartments was determined within masked regions defined by intensity-based segmentation (Slidebook, Intelligent Imaging Innovations, Denver, CO). The contribution to CT fluorescent signal originating from the Golgi/TGN was corrected from the signal in adjacent endosomes by determining the spatial correlation coefficients (r) of fluorescence intensities in both compartments as defined by specific organelle markers. This correction was performed for each time frame of every time-lapse series recorded. The relative fraction of CT localized in the ER was estimated from the fluorescent signal generated within a mask corresponding to the nuclear envelope. About 20 cells per condition were analyzed.

## RESULTS

### *Vesicles and Tubules Transport CT from the Cell Surface to Endosomes before CT Can Access the Golgi Complex*

CT traffic was monitored in BSC1 cells by live-cell confocal microscopy by using a nontoxic CT mutant, E112D, fluorescently labeled with Alexa594. Although most of the entering CT was found in small vesicles moving from the surface to the cell interior, a fraction was detected in tubules (Figure 1A). The tubules seem uniformly labeled with CT and seem to emanate from the plasma membrane. They are long (20–30 $\mu$m) and dynamic, stretching and retracting and pointing toward the perinuclear region (Figure 1A, arrowheads, and Movie 1 in Supplement). Most vesicles and tubules moved bidirectionally along microtubule tracks, as judged by their colocalization with tubulin (Movie 2 and Fig. s1A in Supplement). Consistent with these results, depolymerization of microtubules by nocodazole treatment interfered with the directed motion of the vesicular carriers containing CT and prevented tubule formation (Fig. s1B in Supplement).

We determined that these vesicles and tubules carry CT from the plasma membrane to the cell interior by following the entry of the toxin prebound to the cell surface at 4°C. On warming the cells to 37°C, CT occurred in vesicles and tubules (Figure 1B), confirming the endocytic nature of these carriers. It is unlikely that CT induced the formation of the tubules, because similar results were observed by monitoring the traffic of Bodipy-GM1, a fluorescent analog of the CT receptor (our unpublished data). Internalized CT reached the endosomal compartment before arriving at the Golgi complex. Figure 1, C and D (plots), shows a marked lag

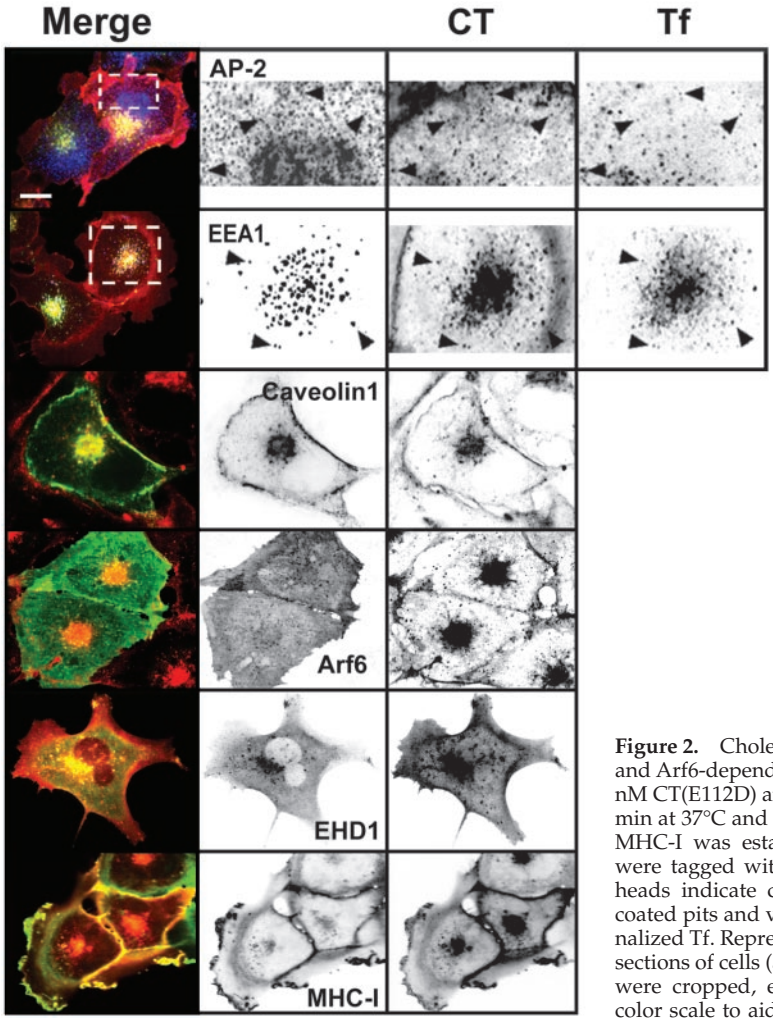


**Figure 2.** Cholera toxin colocalizes with markers of the clathrin-, caveolin-, and Arf6-dependent endocytic pathways. BSC1 cells were incubated with 20 nM CT(E112D) and 50 $\mu$g/ml Alexa 647-hTf for 15 min (top two rows) or 45 min at 37°C and fixed. Colocalization between CT and AP-2, EEA1, Arf6, or MHC-I was established by immunofluorescence. Caveolin 1 and EHD1 were tagged with EGFP and transiently expressed in BSC1 cells. Arrowheads indicate colocalization of CT with AP-2 (presumably in clathrin-coated pits and vesicles), with EEA1 (early endosomes) together with internalized Tf. Representative confocal images from ventral (top row) or middle sections of cells (all others) are shown. Selected regions (stippled-line boxes) were cropped, enlarged, and displayed using an inverted monochrome color scale to aid visualization. Bar, 20 $\mu$m.

phase of 10–15 min before fluorescent CT can be seen to colocalize with the Golgi marker GalT-EGFP.

### *Cholera Toxin Enters through Clathrin-, Caveolin-, and Arf6-dependent Pathways*

To identify entry routes for CT in BSC1 cells, we incubated the cells with this toxin and evaluated the extent of its colocalization with markers specific for the clathrin-, caveolin-, and Arf6-dependent pathways in fixed and live cells. We observed partial colocalization of CT with the clathrin adaptor AP-2 at the cell surface (Figure 2). The clathrin pathway is the main route of entry to the early endosomal compartment. Consistent with the apparent entry of CT via the clathrin pathway, CT was also found in endosomes, colocalizing with endocytosed Tf and with the early endosomal marker EEA1 (Figure 2). However, it is clear that this is not the only entry pathway for CT. CT also colocalized with caveolin found at the cell surface and in the perinuclear region (Figure 2), and with vesicular structures containing Arf6, EHD1, and MHC-I (Figure 2). Together, these static observations are consistent with the possibility that all three of these pathways can mediate CT entry. Indeed, live-cell imaging experiments performed with cells expressing fluorescent protein chimeras of the clathrin light chain A (EYFP-LCA1), caveolin 1 (Cav1-EGFP) (Figure 3), and EHD1 (EGFP-EHD1) (our unpublished data) showed that a fraction of CT follows the dynamics of each of these proteins. For example, in cells expressing Cav1-EGFP we found that CT first binds to the cell surface and is then carried by vesicles or short tubular structures containing caveolin that move toward the perinuclear region (see Movie 3 in Supplement).

### *Inhibiting All Three Identified Entry Pathways Does Not Prevent CT Toxicity*

We assessed the relative contribution of the clathrin-, caveolin-, or Arf6-dependent pathways for CT entry by studying the effects of several inhibitory conditions for these entry pathways alone or in combination. Overexpression of a truncated form of Eps15, Eps15Δ95-295, which blocks entry of Tf through the clathrin pathway (Benmerah *et al.*, 1998, 1999), did not block CT internalization as judged by the ratio of fluorescent signal of CT at the plasma membrane to that in the interior of the cell (Figure 4A). Likewise, treatments known to disrupt the integrity or function of caveolae (Smart *et al.*, 1994; Anderson *et al.*, 1996; Hailstones *et al.*, 1998; Pelkmans *et al.*, 2002), such as incubation with PMA, overexpression of the caveolin mutants Cav1S80E (Figure 4A) cav1(KSF) and cav1(DGI) (our unpublished data), or incubation with genistein (Fig. s6C in Supplement) had minimal effects on CT entry. In contrast, expression of Cav1S80E in 3T3L1 preadipocytes prevented CT entry, presumably

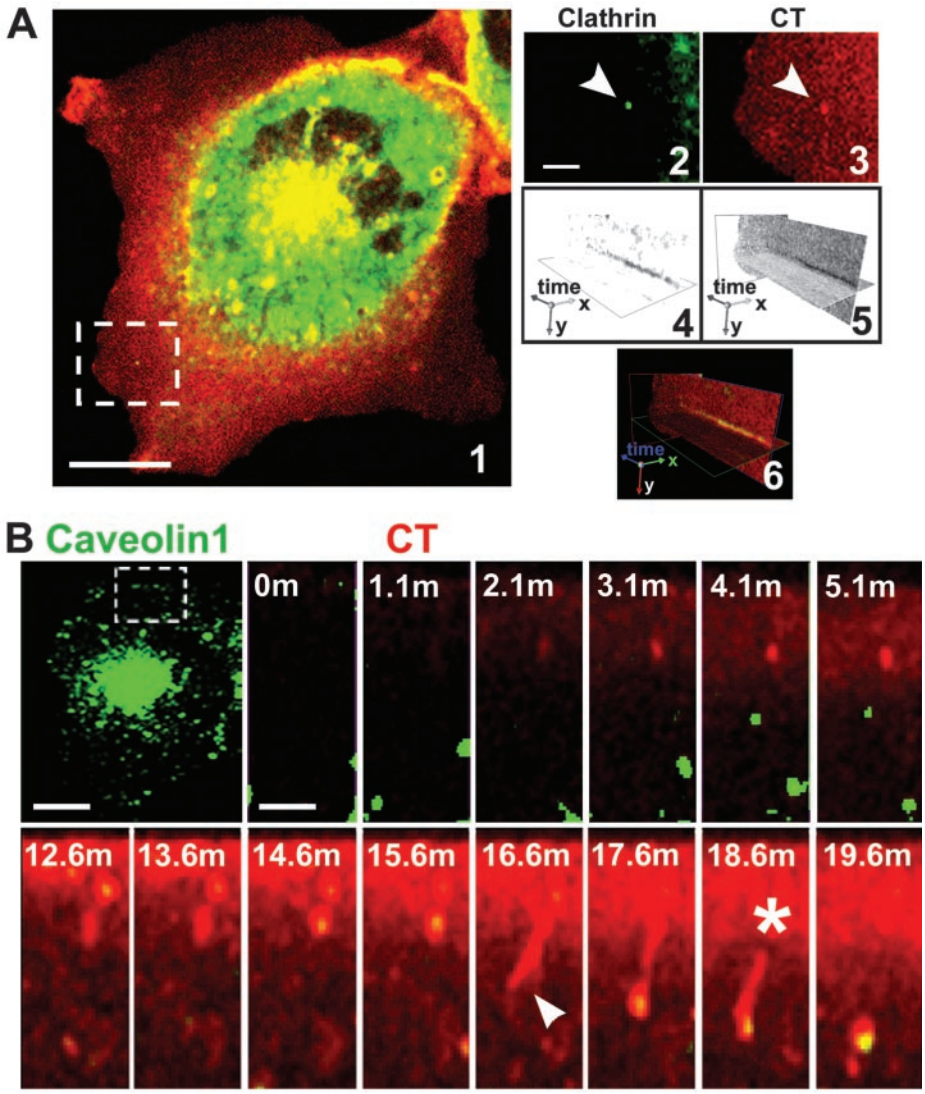


**Figure 3.** Clathrin and caveolin-dependent pathways mediate CT internalization. (A) BSC1 cells stably expressing EYFP-LCA cells were incubated with 20 nM CT(E112D) for 30 min at 37°C, washed, and processed for time-lapse recording. A clathrin-coated pit-like structure, selected from the dorsal cell surface (image 1, stippled-line box, and enlarged in images 2 and 3), containing CT was analyzed with the aid of a kymograph plot for clathrin and toxin content over time (images 4–6). (B) CT(E112D) was added during the time-lapse acquisition to BSC1 cells transiently expressing Cav1-EGFP. The time-lapse series (stippled-line box) shows entry of CT into a caveolin 1-containing tubulo-vesicular structure (Movie 7, a and b). The initial short tubular invagination stretches and eventually disconnects from the cell surface. Bars, 20 $\mu$m (whole cell) and 5 and 3 $\mu$m (cropped regions).

reflecting differences in cell type (Shigematsu *et al.*, 2002). Moreover, overexpression of the Arf6 mutants Arf6Q67L or Arf6T27N, mutants known to prevent the GTP/GDP cycle of this small GTPase (Radhakrishna and Donaldson, 1997) failed to block CT entry (Figure 4A). Similar effects were found using Y-1 adrenal cells instead (Fig. s8 in Supplement). Thus, inhibition of single pathways did not importantly affect CT internalization.

It is possible that CT simultaneously enters through two or all of these pathways. To test this hypothesis, we interfered with two or three of these entry routes at once. We used two distinct methods to simultaneously inhibit the clathrin and caveolin pathways: cholesterol depletion (Hailstones *et al.*, 1998; Rodal *et al.*, 1999; Parpal *et al.*, 2001) and overexpression of DynK44A, a mutant defective in GTP loading and hydrolysis (Herskovits *et al.*, 1993; Vallee *et al.*, 1993; van der Bliek *et al.*, 1993). We found that depletion of cholesterol by incubation with methyl-$\beta$ cyclodextrin did reduce CT entry (Figure 4B), consistent with previous results (Orlandi and Fishman, 1998; Wolf *et al.*, 2002; Le and Nabi, 2003). The effect of DynK44A overexpression was significantly less pronounced (Figure 4B); CT was still able to access the perinuclear region, and more CT tubules occurred, apparently emanating from the plasma membrane, which now contained Tf (Figure 4B), caveolin1-EGFP, Arf6, EHD1, and MHC-I (Fig. s2 in Supplement). To inhibit all these endocytic pathways, we expressed DynK44A together either with Arf6Q67L or Arf6T27N. This caused an essentially complete block of detectable CT internalization in BSC1 and Y-1 cells corresponding to a decrease of at least 100-fold in CT uptake (Figure 4C and s8 in Supplement).

These results indicate that all three of the pathways investigated here are able to carry CT to the cell interior, and only when all of them are blocked does CT entry, either into endosomes or into the Golgi and ER become undetectable. Cholesterol depletion slightly reduced the access of CT to the TGN (~<2-fold) and the ER (>4-fold) (Figure 5) and had a more pronounced effect on its access to the Golgi complex (~12-fold) (Fig. s3 in Supplement), consistent with previous observations (Shogomori and Futerman, 2001; Fujinaga *et al.*, 2003; Le and Nabi, 2003). In contrast, only the combined inhibition of the clathrin, caveolin, and Arf6 pathways blocked the transport of CT to the Golgi and the ER (Figure 4C).

Because CT can only access the cytosol from the ER, we used a functional assay (Maneval *et al.*, 1981; Maenhaut and Libert, 1990; Nambiar *et al.*, 1993) that indirectly measures cAMP levels to verify whether blockade of these three endocytic pathways also reduces CT-elicited toxicity. To do

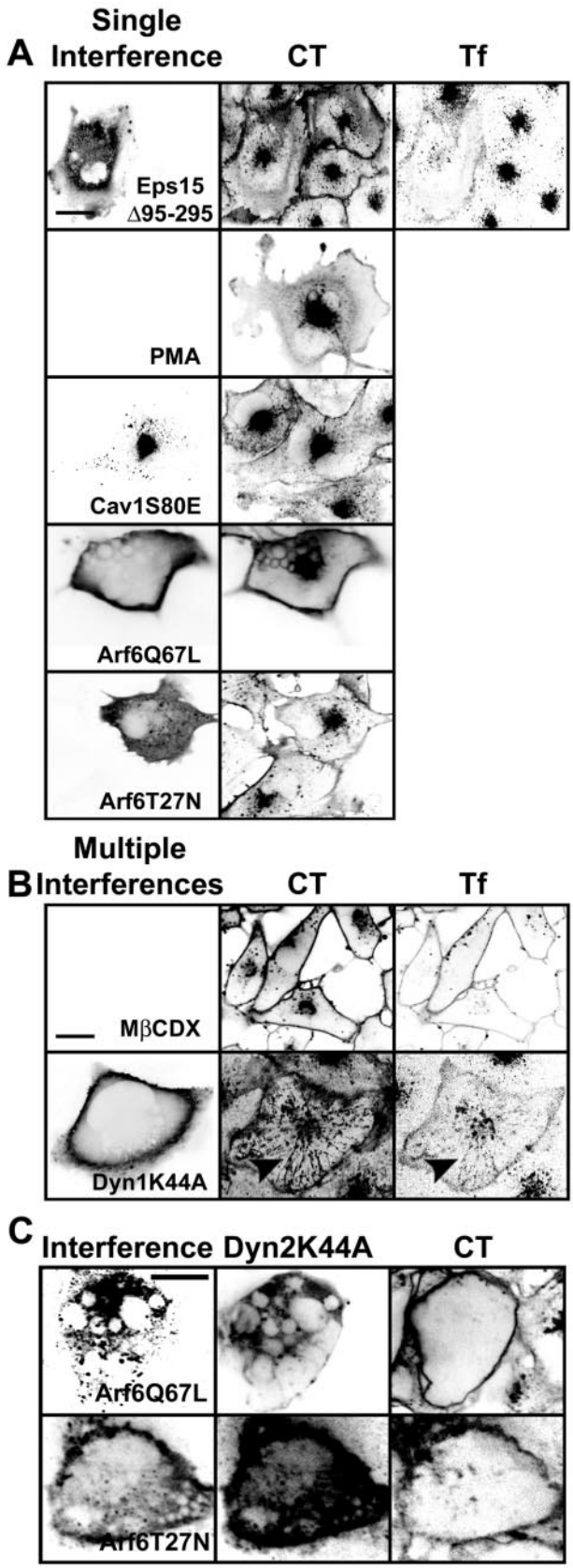


**Figure 4.** Combined inhibition of the clathrin-, caveolin-, and Arf6-dependent pathways strongly inhibits CT entry. (A) Inhibition of clathrin-, caveolin-, or Arf6-dependent pathways has minimal effects on CT entry. Representative images of BSC1 cells transiently expressing EGFP-Eps15Δ95-295, Cav1S80E-myc, Arf6Q67L-HA, Arf6T27N-HA for 24–48 h or treated with 100 nM PMA for 30 min (treatment known to disrupt caveolae) are shown. The block in Tf uptake assessed the inhibition of clathrin-mediated endocytosis; inhibition of caveolin-mediated uptake resulted in a 25% reduction in simian virus 40 infectivity (our unpublished data); and interference with the Arf6-dependent pathway by overexpression of Arf6Q67L resulted in the expected vacuolization of the endosomal compartment (Naslavsky *et al*., 2003). (B) Combined inhibition of clathrin- and caveolin-dependent pathways partially inhibits CT entry. Representative images of BSC1 cells treated with 10 mM methyl-β-cyclodextrin for 30 min or overexpressing Dyn1K44A-HA for 48 h are shown. Under both conditions, Tf uptake was strongly inhibited. Although the retention of CT at the cell surface increased upon cholesterol depletion, and in less degree by interference with dynamin-dependent pathways, its internalization was partially prevented. The number of tubules containing CT increased upon expression of dynamin 1 or 2 K44A mutants, which now contain Tf, Cav1-EGFP, Arf6, EGFP-EHD1, and EGFP-MHC-I (arrowheads and Fig. s2 in Supplement). (C) Coexpression of Dyn2K44A and Arf6Q67L or Arf6T27N strongly prevents CT entry and abolished tubule formation. (A–C) Representative confocal images from middle sections of cells (n = 40–60) displayed using an inverted monochrome scale to aid visualization. Transfected cells were identified by imaging EGFP or by staining for the myc or HA epitopes fused to the corresponding overexpressed proteins. In coexpression of Arf6-HA mutants with DynK44A, we used Dyn2K44A-EGFP. Bars, 20 μm.

this on a single-cell basis, we measured the shape response of Y-1 cells to CT by observing their characteristic cell retraction and appearance of long plasma membrane projections caused by increased intracellular cAMP levels (Figure 6A and Movies 4, a and b, in Supplement). This assay was successfully used to study the trafficking of CT and the effect of different mutations in CT enzymatic activity (Kowal and Srinivasan, 1975; Donta *et al*., 1976; Donta *et al*., 1982; Nambiar *et al*., 1993; Dalsgaard *et al*., 1995; Fontana *et al*., 1995; Wolf *et al*., 1998; Jobling and Holmes, 2001; Morinaga *et al*., 2001) and of its closely related toxin heat-labile LT-II from *Escherichia coli* (Sack and Sack, 1975; Donta *et al*., 1982; Guth *et al*., 1986; Chapman and Daly, 1989; Tauschek *et al*., 2002). Toxin-induced shape changes in this assay depend strictly on toxin trafficking from the plasma membrane to ER where the CT A1-chain retrotranslocates to the cytosol, because neither incubation with 20 nM CT B-subunit alone (Fig. s5B in Supplement) nor incubation with an enzymatically inactive CT mutant (CTE112D) had any toxic effect (Fig. s8 in Supplement). Incubation with forskolin, a direct activator of adenylyl cyclase, used as a positive control in this assay (Donta and Viner, 1975; Donta *et al*., 1976; Maneval *et al*., 1981; Ulaner *et al*., 1999) showed the expected dose-response relationship (Fig. s5A in Supplement). Further confirmation that the change in shape assay reflects increases in intracellular levels of cAMP was obtained by showing a similar response upon incubation of Y-1 cells with the cell-permeable cAMP analogue 8-Br-cAMP (Figure 6B). Overexpression of mutant proteins that block different endocytic routes does not change the normal morphology of the cells (Fig. s4 in Supplement) or their sensitivity to respond to increases in cAMP mediated by increasing amounts of forskolin (Fig. s4 and Fig. s5A in Supplement). This assay shows a dose-response relationship between increasing amounts of CT- and cAMP-induced shape cell changes (Figure 6C). The $EC_{50}$ for CT-induced cell shape change in nontransfected cells is ~32 pM. As shown previously (Stearns *et al*., 1990; Balch *et al*., 1992; Donta *et al*., 1993; Lencer *et al*., 1993; Nambiar *et al*., 1993), extensive disruption of the Golgi complex by treat-

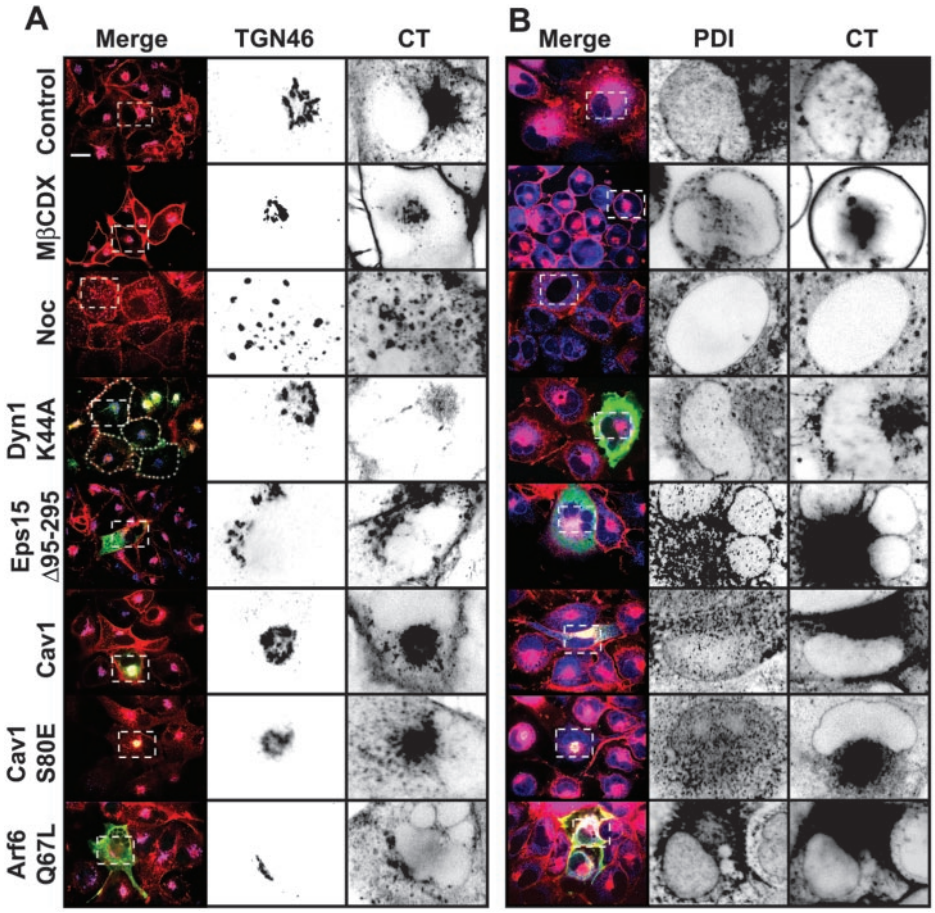


**Figure 5.** Decrease of cholesterol or interference with dynamin function inhibits CT transport to the TGN and the ER. Transport of CT to the TGN (A) and ER (B) in cells subjected to different conditions that perturb endocytosis was assessed by colocalization of the toxin with TGN46 or PDI, respectively. BSC1 cells either expressing the indicated dominant proteins for 24–48 h or treated with nocodazole or methyl-β-cyclodextrin for 30 min were incubated with CT(E112D) for 45 min (A) or 90 min (B) at 37°C. Transfected cells were identified as described in Figure 4. For each condition, representative confocal images are shown (out of at least 50 cells analyzed). Selected regions (stippled-line boxes) of the TGN and ER nuclear envelope were cropped, enlarged, and displayed using an inverted monochrome color scale to facilitate inspection of colocalization. Expression of Dyn1K44A or depletion of cholesterol (by treatment with 10 mM methyl-β-cyclodextrin) significantly reduced CT transport to the TGN and ER, whereas inhibition of single endocytic pathways had no effect. In contrast, microtubule depolymerization (by treatment with 10 μM nocodazole) only inhibited retrograde transport the ER. Bars, 20 μm.

ment with BFA abolished the morphological changes induced by CT (Figure 6A) and also in cells overexpressing Dyn2K44A together with Arf6Q67L (Figure 6D). We conclude that the changes in cell shape are a very sensitive readout to indirectly determine increased levels of cAMP.

We then used this functional assay to study the effect of preventing CT endocytosis in CT-induced toxicity. Unexpectedly, coexpression of Dyn2K44A together with Arf6Q67L or Arf6T27N, conditions that reduced the uptake of fluorescent CT to the endosomes/Golgi/ER below the detection limit of the fluorescent assay (at least a 100-fold reduction in toxin transport; see Figure 4C), showed little or no effect on the rounding of cells treated with 200 pM CT ($EC_{95}$; Figure 6D and Table 1). Moreover, the dose-response curves and $EC_{50}$ values of the cells coexpressing or not the Dynamin and Arf6 mutants were almost indistinguishable (Figure 6C). Thus, normal toxicity is still elicited, even though the concurrent block of the clathrin-, caveolin-, and Arf6-dependent pathways strongly inhibits CT entry and transport to the Golgi and ER determined by visualization of fluorescent CT.

## DISCUSSION

In this study, we find that CT enters cells through the clathrin-, caveolin-, and Arf6-dependent endocytic pathways and that the simultaneous block of all three pathways strongly inhibits the internalization of CT and its access to the Golgi and ER, as assessed by visual inspection of fluorescent CT. The increase in cAMP levels due to CT entry was not affected, however, as determined by the single-cell change-in-shape assay.

Our results are consistent with earlier studies (Parton, 1994; Sofer and Futerman, 1995; Torgersen *et al.*, 2001; Singh *et al.*, 2003) showing that CT enters host cells via multiple routes level but point to different conclusions. In these experiments, perturbations of only one or more endocytic pathway led to a limited reduction in endocytosis and a partial inhibition of CT-induced cAMP production, raising the possibility that the methods used to inhibit endocytosis caused only an incomplete block in toxin uptake by all cells in the assay (upon pharmacological treatment) or complete interference but in only a fraction of cells in the population tested (by overexpression of mutant proteins). Here, using a single-cell assay, we find that CT can enter host cells via multiple routes, some not yet defined at the molecular level. Thus, it is possible that even a complete block of a single endocytic pathway would never be able to inhibit toxicity entirely. Nevertheless, it remains plausible that a particular cell type might use one pathway in preference to others (Singh *et al.*, 2003).

The toxicity assay is highly sensitive to CT ($EC_{50}$ of 32 pM) and has a dynamic range of at least 20-fold in toxin concentration (between 10 and 200 pM). Thus, the assay should readily detect a reduction in the amount of CT reaching the ER as caused by the near complete inhibition of CT transport to the Golgi in cells lacking all three, clathrin-, caveolin-, and Arf6-dependent mechanisms, of endocytosis. If CT endocytosis would only occur through these three routes, then a partial inhibition of 99% in the amount of CT reaching the

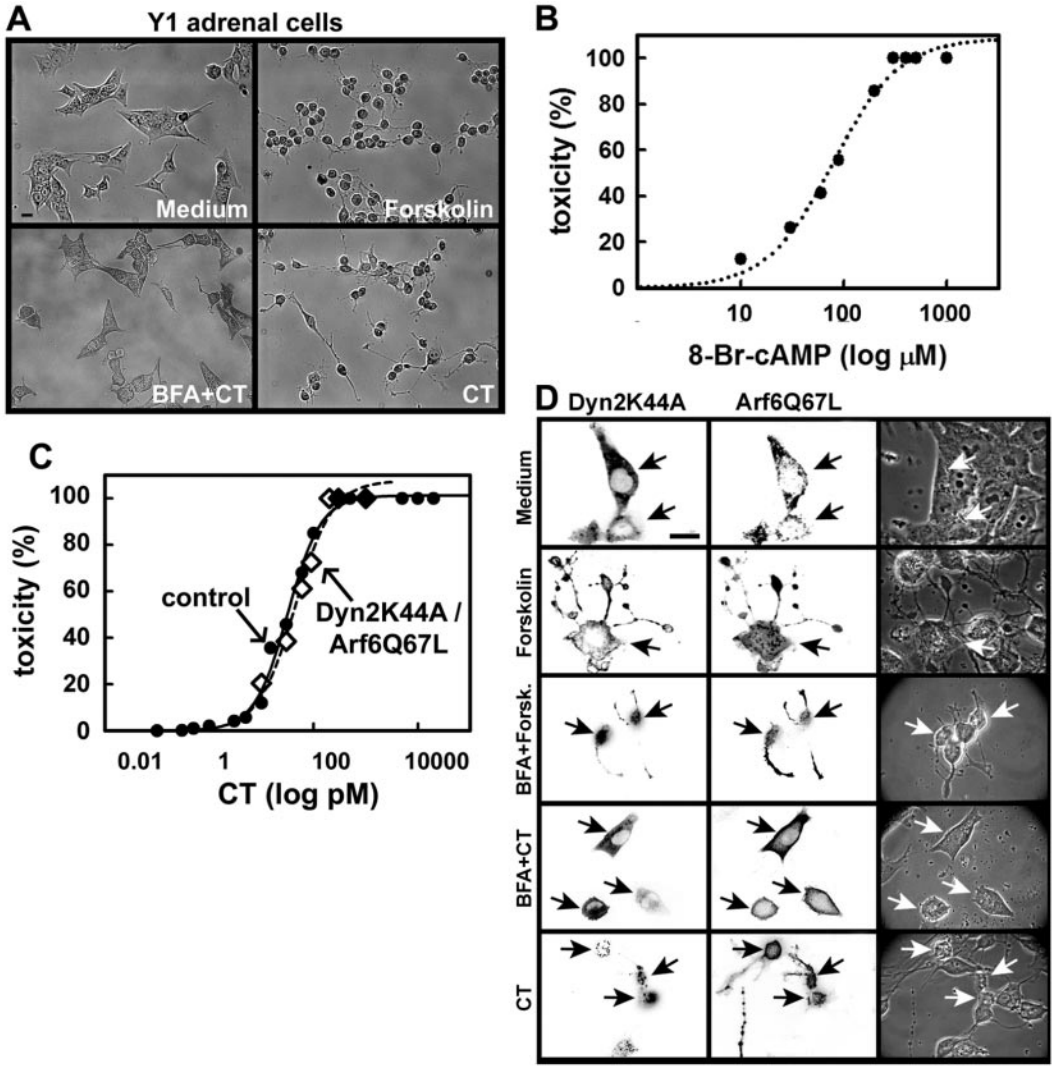


**Figure 6.** CT toxicity does not require active dynamin- and Arf6-dependent endocytic pathways. (A) Assay for toxicity. Incubation of Y-1 mouse adrenal cells with CT (300 pM) or the adenylyl cyclase-agonist forskolin (10 $\mu$M) induces a cAMP-dependent cell shape change characterized by cell retraction, rounding, and the extension of long projections. Pretreatment with BFA (1 $\mu$M) completely inhibits the CT response. Representative phase contrast images were acquired with a 20× lens. B) The shape-change assay used to measure CT-induced toxicity reflects intracellular cAMP levels. On incubation of Y-1 cells with increasing concentrations of the cAMP-permeable analogue 8-Br-cAMP, there is a proportional increase in the number of rounded cells, with an $EC_{50}$ value of ~70 $\mu$M and a linear range between 30 and 140 $\mu$M. At least 500 cells were analyzed per condition. (C) Dose-response curves of CT-induced cell shape change. The $EC_{50}$ for control cells (32 pM, full circles in plot), for cells expressing Dyn2K44A alone (39 pM; our unpublished data) or together with Arf6Q67L (40 pM, empty diamonds in plot) are very similar. At least 350 cells were analyzed per condition. (D) Simultaneous inhibition of the clathrin-, caveolin-, and Arf6-mediated endocytic pathways does not affect CT-induced cell shape change. DynK44A and Arf6 dominant mutants (similar results were obtained with Arf6T27N; our unpublished data) were expressed in Y-1 cells and toxin function assessed by measurement of cell shape change. Representative fluorescence (displayed in inverted monochrome scale) and phase contrast images of cells incubated with medium only, forskolin, BFA in combination with forskolin or CT, and wild-type CT are shown. Expression of these proteins did not alter the normal morphology of Y-1 cells (Fig. s4 in Supplement), or their ability to change upon increased cAMP (Fig. s4 and s5 in Supplement), where cells were incubated with medium with or without forskolin. Cells also were incubated with Tf to verify the block in the clathrin pathway (our unpublished data). Cells were stained with antibodies specific for HA epitope tags to identify Arf6 expression. Bar, 20 $\mu$m.

Golgi/ER (corresponding to our observations) should result in a 2-log increase of the $EC_{50}$ as determined by the dose-response curve (Figure 7). In contrast, our data show that the strong inhibition of all three endocytic pathways has no detectable effect on the toxic response. From these results, we conclude that CT also can enter cells and reach the Golgi and ER through a route that is independent of the clathrin, caveolin, Arf6 pathways (see model in Figure 7).

In favoring this interpretation, it is important to note that the concentration of CT(E112D) (20 nM) used for the direct fluorescence-based traffic assay was >100-fold higher than the concentration of wild-type CT (10–200pM) used in the much more sensitive functional assay. At these lower concentrations, the amount of toxin internalized was below detectable limits as assessed by direct inspection of fluorescent CT. We also examined toxin uptake by indirect immunofluorescence, increasing

**Table 1.** CT-induced change in morphology

| Condition | % Affected cells (n = 150–250, ±5%) |
|---|---|
| Single Interference | |
| Eps15Δ95-295 | 98.5 |
| Cav1S80E | 97.1 |
| Arf6Q67L | 98.4 |
| Arf6T27N | 93.9 |
| Multiple Interferences | |
| Arf6Q67L/Cav1S80E | 88 |
| Eps15Δ95-295/Arf6Q67L | 96 |
| Dyn1K44A | 85 |
| Eps15Δ95-295/Cav1S80E | 96.4 |
| Arf6Q67L/Dyn2K44A | 76.8 |

In each case, the concentration of CT used (of EC95 200 pM) was such that even partial inhibition of endocytic entry should result in a detectable effect on toxicity. In addition, overexpression of two other dominant negative mutants of caveolin or preincubation with genistein did not protect Y-1 cells against CT-induced cell shape changes (Fig. 6A and B). Representative fluorescence (displayed in inverted monochrome scale) and phase contrast images of these conditions are shown in Fig. 7 (Supplement).

the sensitivity of the morphologic assay by 3- to 10-fold. Using this approach, we found no detectable toxin in the ER of cells expressing the dominant negative DynK44A together with Arf6Q67L or Arf6T27N (our unpublished data). Thus, even though the clathrin-, caveolin-, and Arf6-dependent pathways are the main routes for CT entry, they seem not to be the only ones involved in CT transport to the ER. We postulate that there is an unidentified endocytic pathway that remains active in cells expressing DynK44A together with Arf6Q67L or Arf6T27N. This would explain why the toxin remains fully active in cells where the three known mechanisms of endocytosis are blocked. An alternative explanation for the mechanism of toxin access to the ER might be based on the direct fusion of the plasma membrane with the ER, a process recently described in phagocytic cells that occurs during early stages of phagocytosis (Gagnon *et al.*, 2002). Whether this fusion occurs constitutively in all cells, or whether it is sensitive to BFA, however, remains to be determined. Overall, our data are consistent with the existence of another entry pathway relevant for CT activity that is independent of clathrin-, dynamin-, and Arf6-mediated mechanisms.

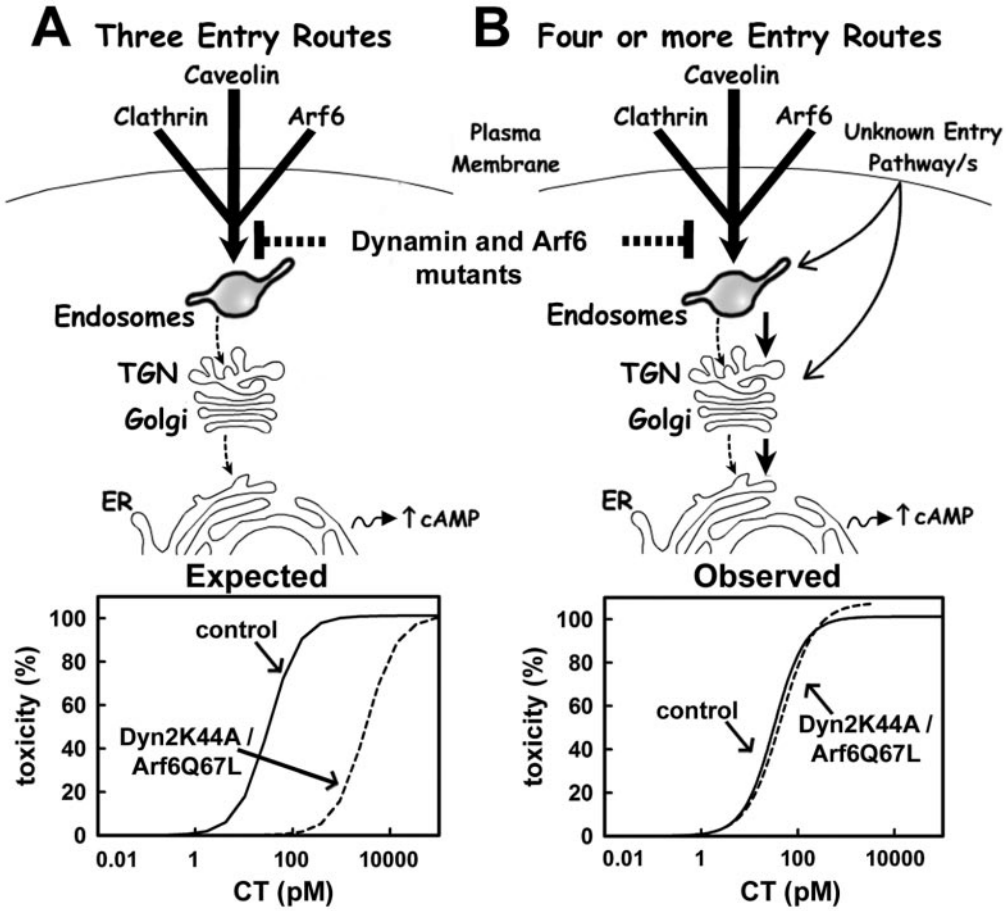


**Figure 7.** Models for delivery routes of CT to the ER. (A) Schematic representation assuming only three routes for CT entry, dependent on clathrin, caveolin, and Arf6 pathways. After arrival of CT to the endosomal compartment, the toxin transverses the Golgi complex and finally arrives to the ER where the CT A1 peptide is retrotranslocated into the cytosol to increase cAMP levels. Inhibition of these three entry routes by coexpression of DynK44A and Arf6 mutants (brackets) reduces CT entry by at least 100-fold. The expected result is a drastic shift in the dose-response relationship of CT toxicity of at least 100-fold. (B) Schematic representation assuming additional routes for CT entry, besides those dependent on the clathrin, caveolin, and Arf6 pathways. In this model, the drastic inhibition in CT entry due to the coexpression of DynK44A and Arf6 mutants does not affect the yet to be determined trafficking pathway(s) used by CT to reach the ER. Under these conditions, transport of CT to the ER is maintained thus resulting in a similar dose-response curve of toxicity.

## ACKNOWLEDGMENTS

We thank Drs. Julie G. Donaldson, Michel Franco, Jeffrey Pessin, Mia Horowitz, Jennifer Lippincott-Schwartz, Hidde Ploegh, and Domenico Tortorella for generously providing DNA constructs and antibodies. We also thank April Griffin for help preparing caveolin mutants; Thomas Nieland and Drs. May Ma, Anan Wu, and Marcelo Ehrlich for helpful discussions; and Dr. Rebecca Ward for editorial assistance. This study was supported in part by DK48106 (to Y.F.) and 1U54AI057159-01(to T.K.).

## REFERENCES

Anderson, H.A., Chen, Y., and Norkin, L.C. (1996). Bound simian virus 40 translocates to caveolin-enriched membrane domains, and its entry is inhibited by drugs that selectively disrupt caveolae. Mol. Biol. Cell *7*, 1825–1834.

Arnaoutova, I., Jackson, C.L., Al-Awar, O.S., Donaldson, J.G., and Loh, Y.P. (2003). Recycling of Raft-associated prohormone sorting receptor carboxypeptidase E requires interaction with ARF6. Mol. Biol. Cell *14*, 4448–4457.

Badizadegan, K., Wolf, A.A., Rodighiero, C., Jobling, M., Hirst, T.R., Holmes, R.K., and Lencer, W.I. (2000). Floating cholera toxin into epithelial cells: functional association with caveolae-like detergent-insoluble membrane microdomains. Int. J. Med. Microbiol. *290*, 403–408.

Balch, W.E., Kahn, R.A., and Schwaninger, R. (1992). ADP-ribosylation factor is required for vesicular trafficking between the endoplasmic reticulum and the cis-Golgi compartment. J. Biol. Chem. *267*, 13053–13061.

Barbieri, J.T., Riese, M.J., and Aktories, K. (2002). Bacterial toxins that modify the actin cytoskeleton. Annu. Rev. Cell Dev. Biol. *18*, 315–344.

Benmerah, A., Bayrou, M., Cerf-Bensussan, N., and Dautry-Varsat, A. (1999). Inhibition of clathrin-coated pit assembly by an Eps15 mutant. J. Cell Sci. *112*, 1303–1311.

Benmerah, A., Lamaze, C., Begue, B., Schmid, S.L., Dautry-Varsat, A., and Cerf-Bensussan, N. (1998). AP-2/Eps15 interaction is required for receptor-mediated endocytosis. J. Cell Biol. *140*, 1055–1062.

Blagoveshchenskaya, A.D., Thomas, L., Feliciangeli, S.F., Hung, C.H., and Thomas, G. (2002). HIV-1 Nef downregulates MHC-I by a PACS-1- and PI3K-regulated ARF6 endocytic pathway. Cell *111*, 853–866.

Brown, F.D., Rozelle, A.L., Yin, H.L., Balla, T., and Donaldson, J.G. (2001). Phosphatidylinositol 4,5-bisphosphate and Arf6-regulated membrane traffic. J. Cell Biol. *154*, 1007–1017.

Caplan, S., Naslavsky, N., Hartnell, L.M., Lodge, R., Polishchuk, R.S., Donaldson, J.G., and Bonifacino, J.S. (2002). A tubular EHD1-containing compartment involved in the recycling of major histocompatibility complex class I molecules to the plasma membrane. EMBO J. *21*, 2557–2567.

Chapman, P.A., and Daly, C.M. (1989). Comparison of Y1 mouse adrenal cell and coagglutination assays for detection of Escherichia coli heat labile enterotoxin. J. Clin. Pathol. *42*, 755–758.

Dalsgaard, A., Albert, M.J., Taylor, D.N., Shimada, T., Meza, R., Serichantalergs, O., and Echeverria, P. (1995). Characterization of *Vibrio cholerae* non-O1 serogroups obtained from an outbreak of diarrhea in Lima, Peru. J. Clin. Microbiol. *33*, 2715–2722.

Diviani, D., and Scott, J.D. (2001). AKAP signaling complexes at the cytoskeleton. J. Cell Sci. *114*, 1431–1437.

Dong, J.M., Leung, T., Manser, E., and Lim, L. (1998). cAMP-induced morphological changes are counteracted by the activated RhoA small GTPase and the Rho kinase ROKalpha. J. Biol. Chem. *273*, 22554–22562.

Donta, S.T., Beristain, S., and Tomicic, T.K. (1993). Inhibition of heat-labile cholera and *Escherichia coli* enterotoxins by brefeldin A. Infect. Immun. *61*, 3282–3286.

Donta, S.T., Kreiter, S.R., and Wendelschafer-Crabb, G. (1976). Morphological and steroidogenic changes in cultured adrenal tumor cells induced by a subunit of cholera enterotoxin. Infect. Immun. *13*, 1479–1482.

Donta, S.T., Poindexter, N.J., and Ginsberg, B.H. (1982). Comparison of the binding of cholera and *Escherichia coli* enterotoxins to Y1 adrenal cells. Biochemistry *21*, 660–664.

Donta, S.T., and Viner, J.P. (1975). Inhibition of the steroidogenic effects of cholera and heat-labile Escherichia coli enterotoxins by GM1 ganglioside: evidence for a similar receptor site for the two toxins. Infect. Immun. *11*, 982–985.

Falguieres, T., Mallard, F., Baron, C., Hanau, D., Lingwood, C., Goud, B., Salamero, J., and Johannes, L. (2001). Targeting of Shiga toxin B-subunit to retrograde transport route in association with detergent-resistant membranes. Mol. Biol. Cell *12*, 2453–2468.

Fishman, P.H., and Atikkan, E.E. (1980). Mechanism of action of cholera toxin: effect of receptor density and multivalent binding on activation of adenylate cyclase. J. Membr. Biol. *54*, 51–60.

Fontana, M.R., Manetti, R., Giannelli, V., Magagnoli, C., Marchini, A., Olivieri, R., Domenighini, M., Rappuoli, R., and Pizza, M. (1995). Construction of nontoxic derivatives of cholera toxin and characterization of the immunological response against the A subunit. Infect Immun. *63*, 2356–2360.

Fujinaga, Y., Wolf, A.A., Rodighiero, C., Wheeler, H., Tsai, B., Allen, L., Jobling, M.G., Rapoport, T., Holmes, R.K., and Lencer, W.I. (2003). Gangliosides that associate with lipid rafts mediate transport of cholera and related toxins from the plasma membrane to ER. Mol. Biol. Cell *14*, 4783–4793.

Gagnon, E., Duclos, S., Rondeau, C., Chevet, E., Cameron, P.H., Steele-Mortimer, O., Paiement, J., Bergeron, J.J., and Desjardins, M. (2002). Endoplasmic reticulum-mediated phagocytosis is a mechanism of entry into macrophages. Cell *110*, 119–131.

Guerrant, R.L., Brunton, L.L., Schnaitman, T.C., Rebhun, L.I., and Gilman, A.G. (1974). Cyclic adenosine monophosphate and alteration of Chinese hamster ovary cell morphology: a rapid, sensitive in vitro assay for the enterotoxins of *Vibrio cholerae* and *Escherichia coli*. Infect. Immun. *10*, 320–327.

Guth, B.E., Twiddy, E.M., Trabulsi, L.R., and Holmes, R.K. (1986). Variation in chemical properties and antigenic determinants among type II heat-labile enterotoxins of *Escherichia coli*. Infect. Immun. *54*, 529–536.

Hagmann, J., and Fishman, P.H. (1982). Detergent extraction of cholera toxin and gangliosides from cultured cells and isolated membranes. Biochim. Biophys. Acta *720*, 181–187.

Hailstones, D., Sleer, L.S., Parton, R.G., and Stanley, K.K. (1998). Regulation of caveolin and caveolae by cholesterol in MDCK cells. J. Lipid Res. *39*, 369–379.

Herskovits, J.S., Burgess, C.C., Obar, R.A., and Vallee, R.B. (1993). Effects of mutant rat dynamin on endocytosis. J. Cell Biol. *122*, 565–578.

Jobling, M.G., and Holmes, R.K. (2001). Biological and biochemical characterization of variant A subunits of cholera toxin constructed by site-directed mutagenesis. J. Bacteriol. *183*, 4024–4032.

Joseph, K.C., Kim, S.U., Stieber, A., and Gonatas, N.K. (1978). Endocytosis of cholera toxin into neuronal GERL. Proc. Natl. Acad. Sci. USA *75*, 2815–2819.

Joseph, K.C., Stieber, A., and Gonatas, N.K. (1979). Endocytosis of cholera toxin in GERL-like structures of murine neuroblastoma cells pretreated with GM1 ganglioside. Cholera toxin internalization into Neuroblastoma GERL. J. Cell Biol. *81*, 543–554.

Kahn, R.A., and Gilman, A.G. (1984). ADP-ribosylation of Gs promotes the dissociation of its alpha and beta subunits. J. Biol. Chem. *259*, 6235–6240.

Kassis, S., and Fishman, P.H. (1982). Different mechanisms of desensitization of adenylate cyclase by isoproterenol and prostaglandin E1 in human fibroblasts. Role of regulatory components in desensitization. J. Biol. Chem. *257*, 5312–5318.

Kassis, S., Hagmann, J., Fishman, P.H., Chang, P.P., and Moss, J. (1982). Mechanism of action of cholera toxin on intact cells. Generation of A1 peptide and activation of adenylate cyclase. J. Biol. Chem. *257*, 12148–12152.

Kirchhausen, T., Scarmato, P., Harrison, S.C., Monroe, J.J., Chow, E.P., Mattaliano, R.J., Ramachandran, K.L., Smart, J.E., Ahn, A.H., and Brosius, J. (1987). Clathrin light chains LCA and LCB are similar, polymorphic, and share repeated heptad motifs. Science *236*, 320–324.

Kowal, J., and Fiedler, R.P. (1969). Adrenal cells in tissue culture. II. Steroidogenic responses to nucleosides and nucleotides. Endocrinology *84*, 1113–1117.

Kowal, J., and Srinivasan, S. (1975). Adrenal cells in tissue culture the effects of choleragen and ACTH on steroid and cyclic-AMP metabolism. Endocr. Res. Commun. *2*, 65–86.

Larsen, J.E., Massol, R.H., Nieland, T.J., and Kirchhausen, T. (2004). HIV Nef-mediated major histocompatibility complex class I down-modulation is independent of Arf6 activity. Mol. Biol. Cell *15*, 323–331.

Le, P.U., and Nabi, I.R. (2003). Distinct caveolae-mediated endocytic pathways target the Golgi apparatus and the endoplasmic reticulum. J. Cell Sci. *116*, 1059–1071.

Lencer, W.I., Constable, C., Moe, S., Jobling, M.G., Webb, H.M., Ruston, S., Madara, J.L., Hirst, T.R., and Holmes, R.K. (1995). Targeting of cholera toxin and Escherichia coli heat labile toxin in polarized epithelia: role of COOH-terminal KDEL. J. Cell Biol. *131*, 951–962.

Lencer, W.I., de Almeida, J.B., Moe, S., Stow, J.L., Ausiello, D.A., and Madara, J.L. (1993). Entry of cholera toxin into polarized human intestinal epithelial cells. Identification of an early brefeldin A sensitive event required for A1-peptide generation. J. Clin. Investig. *92*, 2941–2951.

Luetterforst, R., Stang, E., Zorzi, N., Carozzi, A., Way, M., and Parton, R.G. (1999). Molecular characterization of caveolin association with the Golgi complex: identification of a cis-Golgi targeting domain in the caveolin molecule. J. Cell Biol. *145*, 1443–1459.

Maenhaut, C., and Libert, F. (1990). An efficient screening morphological test for the identification and characterization of cyclic AMP-coupled hormone receptors. Exp. Cell Res. *187*, 104–110.

Majoul, I., Sohn, K., Wieland, F.T., Pepperkok, R., Pizza, M., Hillemann, J., and Soling, H.D. (1998). KDEL receptor (Erd2p)-mediated retrograde transport of the cholera toxin A subunit from the Golgi involves COPI, p23, and the COOH terminus of Erd2p. J. Cell Biol. *143*, 601–612.

Majoul, I.V., Bastiaens, P.I., and Soling, H.D. (1996). Transport of an external Lys-Asp-Glu-Leu (KDEL) protein from the plasma membrane to the endoplasmic reticulum: studies with cholera toxin in Vero cells. J. Cell Biol. *133*, 777–789.

Maneval, D.R., Colwell, R.R., Grays, S.W.J., and Donta, S.T. (1981). A tissue culture method for the detection of bacterial enterotoxins. J. Tissue Cult. Methods *6*, 85–90.

Mobius, W., Herzog, V., Sandhoff, K., and Schwarzmann, G. (1999). Intracellular distribution of a biotin-labeled ganglioside, GM1, by immunoelectron microscopy after endocytosis in fibroblasts. J. Histochem. Cytochem. *47*, 1005–1014.

Montecucco, C. (1998). Protein toxins and membrane transport. Curr. Opin. Cell Biol. *10*, 530–536.

Montesano, R., Roth, J., Robert, A., and Orci, L. (1982). Non-coated membrane invaginations are involved in binding and internalization of cholera and tetanus toxins. Nature *296*, 651–653.

Morinaga, N., Kaihou, Y., Vitale, N., Moss, J., and Noda, M. (2001). Involvement of ADP-ribosylation factor 1 in cholera toxin-induced morphological changes of Chinese hamster ovary cells. J. Biol. Chem. *276*, 22838–22843.

Moss, J., and Vaughan, M. (1988). ADP-ribosylation of guanyl nucleotide-binding regulatory proteins by bacterial toxins. Adv. Enzymol. Relat. Areas Mol. Biol. *61*, 303–379.

Nambiar, M.P., Oda, T., Chen, C., Kuwazuru, Y., and Wu, H.C. (1993). Involvement of the Golgi region in the intracellular trafficking of cholera toxin. J. Cell Physiol. *154*, 222–228.

Naslavsky, N., Weigert, R., and Donaldson, J.G. (2003). Convergence of non-clathrin- and clathrin-derived endosomes involves Arf6 inactivation and changes in phosphoinositides. Mol. Biol. Cell *14*, 417–431.

Nichols, B.J. (2002). A distinct class of endosome mediates clathrin-independent endocytosis to the Golgi complex. Nat. Cell Biol. *4*, 374–378.

Nichols, B.J., Kenworthy, A.K., Polishchuk, R.S., Lodge, R., Roberts, T.H., Hirschberg, K., Phair, R.D., and Lippincott-Schwartz, J. (2001). Rapid cycling of lipid raft markers between the cell surface and Golgi complex. J. Cell Biol. *153*, 529–541.

Orlandi, P.A., Curran, P.K., and Fishman, P.H. (1993). Brefeldin A blocks the response of cultured cells to cholera toxin. Implications for intracellular trafficking in toxin action. J. Biol. Chem. *268*, 12010–12016.

Orlandi, P.A., and Fishman, P.H. (1998). Filipin-dependent inhibition of cholera toxin: evidence for toxin internalization and activation through caveolae-like domains. J. Cell Biol. *141*, 905–915.

Parpal, S., Karlsson, M., Thorn, H., and Stralfors, P. (2001). Cholesterol depletion disrupts caveolae and insulin receptor signaling for metabolic control via insulin receptor substrate-1, but not for mitogen-activated protein kinase control. J. Biol. Chem. *276*, 9670–9678.

Parton, R.G. (1994). Ultrastructural localization of gangliosides; GM1 is concentrated in caveolae. J. Histochem. Cytochem. *42*, 155–166.

Pelkmans, L., Kartenbeck, J., and Helenius, A. (2001). Caveolar endocytosis of simian virus 40 reveals a new two-step vesicular-transport pathway to the ER. Nat. Cell Biol. *3*, 473–483.

Pelkmans, L., Puntener, D., and Helenius, A. (2002). Local actin polymerization and dynamin recruitment in SV40-induced internalization of caveolae. Science *296*, 535–539.

Radhakrishna, H., and Donaldson, J.G. (1997). ADP-ribosylation factor 6 regulates a novel plasma membrane recycling pathway. J. Cell Biol. *139*, 49–61.

Rodal, S.K., Skretting, G., Garred, O., Vilhardt, F., van Deurs, B., and Sandvig, K. (1999). Extraction of cholesterol with methyl-beta-cyclodextrin perturbs formation of clathrin-coated endocytic vesicles. Mol. Biol. Cell *10*, 961–974.

Sack, D.A., and Sack, R.B. (1975). Test for enterotoxigenic *Escherichia coli* using Y-1 adrenal cells in miniculture. Infect. Immun. *11*, 334–336.

Sandvig, K., and van Deurs, B. (2002a). Membrane traffic exploited by protein toxins. Annu. Rev. Cell Dev. Biol. *18*, 1–24.

Sandvig, K., and van Deurs, B. (2002b). Transport of protein toxins into cells: pathways used by ricin, cholera toxin and Shiga toxin. FEBS Lett. *529*, 49–53.

Schafer, D.E., Lust, W.D., Sircar, B., and Goldberg, N.D. (1970). Elevated concentration of adenosine 3′:5′-cyclic monophosphate in intestinal mucosa after treatment with cholera toxin. Proc. Natl. Acad. Sci USA *67*, 851–856.

Schmitz, A., Herrgen, H., Winkeler, A., and Herzog, V. (2000). Cholera toxin is exported from microsomes by the Sec61p complex. J. Cell Biol. *148*, 1203–1212.

Scott, J.D. (2003). A-kinase-anchoring proteins and cytoskeletal signalling events. Biochem. Soc. Trans. *31*, 87–89.

Seamon, K.B., and Daly, J.W. (1981). Forskolin: a unique diterpene activator of cyclic AMP-generating systems. J. Cyclic Nucleotide Res. *7*, 201–224.

Seamon, K.B., Padgett, W., and Daly, J.W. (1981). Forskolin: unique diterpene activator of adenylate cyclase in membranes and in intact cells. Proc. Natl. Acad. Sci. USA *78*, 3363–3367.

Shigematsu, S., Watson, R.T., Khan, A.H., and Pessin, J.E. (2002). The adipocyte plasma membrane caveolin functional/structural organization is necessary for the efficient endocytosis of GLUT4. J. Biol. Chem. *278*, 10683–10690.

Shogomori, H., and Futerman, A.H. (2001). Cholera toxin is found in detergent-insoluble rafts/domains at the cell surface of hippocampal neurons but is internalized via a raft-independent mechanism. J. Biol. Chem. *276*, 9182–9188.

Singh, R.D., Puri, V., Valiyaveettil, J.T., Marks, D.L., Bittman, R., and Pagano, R.E. (2003). Selective caveolin-1-dependent endocytosis of glycosphingolipids. Mol. Biol. Cell *14*, 3254–3265.

Smart, E.J., Foster, D.C., Ying, Y.S., Kamen, B.A., and Anderson, R.G. (1994). Protein kinase C activators inhibit receptor-mediated potocytosis by preventing internalization of caveolae. J. Cell Biol. *124*, 307–313.

Sofer, A., and Futerman, A.H. (1995). Cationic amphiphilic drugs inhibit the internalization of cholera toxin to the Golgi apparatus and the subsequent elevation of cyclic AMP. J. Biol. Chem. *270*, 12117–12122.

Spangler, B.D. (1992). Structure and function of cholera toxin and the related Escherichia coli heat-labile enterotoxin. Microbiol. Rev. *56*, 622–647.

Stearns, T., Willingham, M.C., Botstein, D., and Kahn, R.A. (1990). ADP-ribosylation factor is functionally and physically associated with the Golgi complex. Proc. Natl. Acad. Sci. USA *87*, 1238–1242.

Tauschek, M., Gorrell, R.J., Strugnell, R.A., and Robins-Browne, R.M. (2002). Identification of a protein secretory pathway for the secretion of heat-labile enterotoxin by an enterotoxigenic strain of *Escherichia coli*. Proc. Natl. Acad. Sci. USA *99*, 7066–7071.

Torgersen, M.L., Skretting, G., van Deurs, B., and Sandvig, K. (2001). Internalization of cholera toxin by different endocytic mechanisms. J. Cell Sci. *114*, 3737–3747.

Tran, D., Carpentier, J.L., Sawano, F., Gorden, P., and Orci, L. (1987). Ligands internalized through coated or noncoated invaginations follow a common intracellular pathway. Proc. Natl. Acad. Sci. USA *84*, 7957–7961.

Tsai, B., Gilbert, J.M., Stehle, T., Lencer, W., Benjamin, T.L., and Rapoport, T.A. (2003). Gangliosides are receptors for murine polyoma virus and SV40. EMBO J. *22*, 4346–4355.

Tsai, B., Rodighiero, C., Lencer, W.I., and Rapoport, T.A. (2001). Protein disulfide isomerase acts as a redox-dependent chaperone to unfold cholera toxin. Cell *104*, 937–948.

Tsai, B., Ye, Y., and Rapoport, T.A. (2002). Retro-translocation of proteins from the endoplasmic reticulum into the cytosol. Nat. Rev. Mol. Cell. Biol. *3*, 246–255.

Ulaner, G.A., Chuang, J., Lin, W., Woodbury, D., Myers, R.V., and Moyle, W.R. (1999). Desensitization and resensitization of lutropin receptors expressed in transfected Y-1 adrenal cells. J. Endocrinol. *163*, 289–297.

Vallee, R.B., Herskovits, J.S., Aghajanian, J.G., Burgess, C.C., and Shpetner, H.S. (1993). Dynamin, a GTPase involved in the initial stages of endocytosis. Ciba Found. Symp. *176*, 185–193; discussion 193–187.

van der Bliek, A.M., Redelmeier, T.E., Damke, H., Tisdale, E.J., Meyerowitz, E.M., and Schmid, S.L. (1993). Mutations in human dynamin block an intermediate stage in coated vesicle formation. J. Cell Biol. *122*, 553–563.

Van Dop, C., Tsubokawa, M., Bourne, H.R., and Ramachandran, J. (1984). Amino acid sequence of retinal transducin at the site ADP-ribosylated by cholera toxin. J. Biol. Chem. *259*, 696–698.

Wolf, A.A., Fujinaga, Y., and Lencer, W.I. (2002). Uncoupling of the cholera toxin-G(M1) ganglioside receptor complex from endocytosis, retrograde Golgi trafficking, and downstream signal transduction by depletion of membrane cholesterol. J. Biol. Chem. *277*, 16249–16256.

Wolf, A.A., Jobling, M.G., Wimer-Mackin, S., Ferguson-Maltzman, M., Madara, J.L., Holmes, R.K., and Lencer, W.I. (1998). Ganglioside structure dictates signal transduction by cholera toxin and association with caveolae-like membrane domains in polarized epithelia. J. Cell Biol. *141*, 917–927.